Geomechanical characterization of mud volcanoes using P-wave velocity datasets

DOI:
10.1144/SP458.2

Document Version
Accepted author manuscript

Geomechanical characterization of mud volcanoes using P-wave velocity datasets

RASHAD GULMAMMADOV, STEPHEN COVEY-CRUMP, MADS HUUSE

School of Earth and Environmental Sciences, University of Manchester, Manchester, M13 9PL, U.K.

**Corresponding author (e-mail: rashad.gulmammadov@alumni.manchester.ac.uk)*

Abstract: Mud volcanoes occur in many petroliferous basins and are associated with significant drilling hazards. To illustrate the type of information that can be extracted from limited petrophysical datasets in such geomechanically complex settings, we use P-wave velocity data to calculate mechanical properties and stresses on a 2D vertical section across a mud volcano in the Azeri-Chirag-Guneshly field, South Caspian Basin. We find (a) that the values of the properties and stresses calculated in this way have realistic magnitudes, (b) that the calculated pore fluid pressures show spatial variations around the mud volcano which potentially highlight areas of fluid recharging after the most recent eruption, and (c) that the information obtained is sufficient to provide helpful indications of the width of the drilling window. While calculations of this kind may be readily improved with more sophisticated petrophysical datasets, the simplicity of the approach we use makes it attractive for reconnaissance surveys designed to identify targets worthy of further investigation in developing our understanding of mud volcano geomechanics or which could be used to help formulate drilling strategies.

To date around 6500 mud volcanoes have been identified worldwide, both onshore and offshore (Judd 2005). They are primarily developed where mudstone sequences are overlain by thick and rapidly deposited sands from modern and Tertiary deltas, for example, the Volga in the South Caspian Basin, the Baram in Borneo, the Niger in West Africa, the Mississippi in the U.S.A., and the Mackenzie in Arctic Canada (Allen & Allen 2013). Their occurrence is generally associated with an active tectonic setting, rapid sedimentation and high rates of gas generation (Milkov 2000).

As pathways for fluid release from deeply buried and overpressured sedimentary successions, mud volcanoes in petroliferous basins are important features to consider in reducing the risk and uncertainty within different parts of the Exploration & Production cycle. Their feeder pipes may rupture the seal and allow hydrocarbon fluids and entrained sediment to migrate up through the sealing sequences (Cartwright et al. 2007; Hong et al. 2013). This does not necessarily imply total failure of the seal because it is the timing and efficiency of mud volcano eruptions relative to the timing of petroleum charging that defines the failure level of the seal (Cartwright et al. 2007). Indeed in many cases petroleum accumulations are discovered because of seal breach and the subsequent leaking of hydrocarbon rich fluids to the surface at the sites of mud volcanoes (Clarke & Cleverly 1991). Nevertheless, the presence of mud volcanoes and the scale, geometry and activity of the plumbing systems beneath them are clearly important factors to consider when formulating strategies for field development and the siting of the facilities.

For these reasons, among others, mud volcanoes have been systematically studied worldwide to develop an understanding of (a) the controls on their internal structure and geomorphology (Hovland et al. 1997; Dimitrov 2002; Deville et al. 2003; Evans et al. 2007; Soto et al. 2011), (b) the structural controls on mud volcano locations (Roberts et al. 2011; Bonini 2013), (c) fluid/sediment flow under mud volcano complexes (Planke et al. 2003; Calvès et al. 2008), (d) the factors influencing the severity of mud volcano eruptions (Lerche & Bagirov 1999; Kopf et al. 2009; Contet & Uterseh 2015; Hill et al. 2015), and (e) controls on the geochemistry of the erupted fluids (Azzaro et al. 1993; Mazzini et al 2009; Bristow et al. 2000; Feseker et al. 2010; Oppo et al. 2014). In offshore areas, numerous multi-scale near-surface geological studies have been performed to mitigate the risks to seabed facilities that are associated with mud volcano activity and its accompanying hazardous phenomena, such as the presence of shallow gas, slope failure and pockmarks (Hill et al. 2015; Contet & Unterseh 2015; Unterseh & Contet 2015). Yet the extent to which drilling in such zones has to be avoided because of mud volcano related risks remains unclear.

Among the challenges posed by the complicated geology in and around mud volcanoes is the prediction of local pore fluid pressures which has significant implications for drilling (e.g. borehole blowouts and instability). Understanding these manifestations of localized fluid flow from a geomechanical perspective requires an analysis of the fluid and pressure distribution, the deformation history, the distribution of fractures, and the state of stress around the mud volcano. This, in turn, requires comprehensive petrophysical datasets and sophisticated data analysis. However, within these geomechanically complex areas there remains value in adopting a simpler reconnaissance-type approach in order to identify targets for more detailed investigation and key features that require a better understanding.

In this paper, we use P-wave velocity data available in the public domain to estimate the mechanical properties and stresses on a 2D vertical section across a mud volcano structure located in the Azeri part of the Azeri-Chirag-Guneshly (ACG) field, South Caspian Basin (SCB). The aim of the study is to determine whether useful geomechanical information can be extracted from such a limited dataset.

Geological setting

Regional geology

The South Caspian Basin, offshore Azerbaijan (Fig. 1a), is a deep Tertiary basin, characterized by mobilized overpressured sediments that cause instability on the basin margins and in deeper strata. The initiation of the basin corresponds to closure of the Tethys Ocean as a result of Arabia-Eurasia convergence (Kopf et al. 2009; Morton et al. 2003). Subduction of the Arabian plate under Eurasia to the NNE generated an accretionary prism during the Mesozoic/Early Tertiary. Following closure of Tethys (~20Ma), continuing convergence and uplift to the north led to folding of a thick Oligocene to Holocene sequence deposited in front of the previously active accretionary prism (Jackson et al. 2002; Stewart & Davies. 2006; Santos Betancor & Soto 2015) (Fig. 1b). Along the northern margin of the basin, anticlinal structures developed within the NW-SE trending Absheron-Balkhan deep-seated structural uplift, which is the offshore extension of the Caucasus fold belt (Fig. 1a).

The sedimentary succession in the basin (Fig. 2) mainly comprises Cenozoic clastic sediments deposited within three large delta systems: Kura from the west (sediments from Lesser Caucasus), Amu Darya from the east (sediments from Balkhans) and Volga from the north (sediments from Greater Caucasus and Urals) (Bredehoeft et al. 1988;

Smith-Rouch 2006). These were deposited at remarkably high rates (up to 2.4 km Myr^{-1}) as the basin subsided, generating a sedimentary succession that is over 25 km thick (Lerche & Bagirov 1999). A cover sequence, up to 10 km thick, comprising sand-silt-shale intercalations, was deposited during the Pliocene and Quaternary. The main source rock for the extensive hydrocarbon reserves within the basin is the Maykop, a kilometre thick sequence of organic-rich mudstones deposited during the Oligocene and Early Miocene (Abrams et al. 1997; Jones et al. 1997). The main producing unit, both onshore and offshore in the SCB, is the overlying Productive Series deposited during the Late Miocene to Early Pliocene. This succession is composed of alternating, regionally extensive, fluvio-deltaic sandstones, separated by laterally extensive lacustrine shales. The lacustrine shales act as major pressure seals within the basin (Javanshir et al. 2015).

Within the South Caspian Basin rapid sediment burial has led to small geothermal gradients (13-18 °C km^{-1}), setting the hydrocarbon generation depth at 5-10 km in the western shelf and continental slope, and 6-14 km in the deep-water region (Guliyev et al. 2011). The presence of low permeability seals coupled with the high rate of gas generation, means that within the mudstone units there are abnormally high pore fluid pressures. Pore fluid pressures in shales enclosing the regionally developed reservoirs are estimated to exceed hydrostatic pressures by a factor of ~1.8, whereas in sandstones within the basin the difference is a factor of ~1.4 (Bredehoeft et al. 1988).

The high rate of sedimentation and gas generation in the basin resulted in slow pore fluid removal from the compacting mudstones during the burial and this has led to a high level of under-compaction (Buryakovsky et al. 2001). These geological conditions, coupled with the active tectonic regime, present a wide range of geological hazards for oil and gas operations (Lerche & Bagirov 1999). Among these are mud flows and gas emissions that can damage rigs and production equipment, hydrate dissociation which is hazardous for drilling activities, and the presence of submarine banks that are dangerous to marine traffic. In addition to the natural hazards that are present on the seabed and at shallow subsurface depths, significant challenges for drilling processes are presented at greater depths by deep earthquakes and areas of large fluid overpressure.

ACG field

The ACG field complex is located within anticlinal structures on the northern boundary of the South Caspian Basin at water depths of 95-425 m (Fig. 1a). The cores of these anticlines contain mobile shales from the Maykop sequence – the depth to the top of this sequence is ~5 km in the ACG. Where this mobile shale has exploited zones of weakness, mud volcanoes have formed resulting in the expulsion of mud and fluids, including hydrocarbons, at the seabed. These mud volcanoes are developed within three anticlinal culminations: Azeri, Chirag and Guneshly (Hill et al. 2015). Of these, the Chirag mud volcano is the most extensively studied (e.g. Lerche & Bagirov 1999; Stewart & Davies 2006).

The key geometric parameters and mechanical conditions of the Chirag mud volcano are illustrated in Figure 3. This mud volcano is located at a water depth of 120 m, and contains several buried mud cones that are stacked vertically but share a common root system (Stewart & Davies 2006). The eruptive mud originates from the Maykop and is composed primarily of montmorillonite clay with some volcanic ash (Buryakovsky et al. 2001; Evans et al. 2006). Geochemical evidence suggests that the fluids within the mud volcano plumbing system also derive primarily from the Maykop (Mazzini et al. 2008; Kopf et al. 2009) but with a contribution from the Productive Series (Lerche & Bagirov 1999; Javanshir et al. 2015).

The pore fluid pressure gradients in the area are typically 0.0120 MPa/m (Buryakovsky et al. 1995). Fluid overpressure in the area is generally associated with disequilibrium (gravitational) compaction. The smectite-illite transformation occurs at temperatures of 75°-150°C, corresponding to depths of >7 km (Feyzullayev & Lerche 2009).

Based on the eruption statistics for onshore mud volcanoes in Azerbaijan, it is estimated that mean waiting time for weak eruptions of the Chirag mud volcano is 95 years and 272 years for the average and strong eruptions, respectively (Lerche & Bagirov 1999). High resolution geophysical imagery is currently being used to monitor hydrocarbon seepage, mud flows and the formation of slope failure scars in order to provide a better understanding of the activity of this mud volcano (Hill et al. 2015; Unterseh & Contet 2015).

Modelling background

Analytical and empirical correlations used in this study

Several analytical and empirical correlations between P-wave velocity and mechanical properties / in-situ stresses have been developed which allow the latter to be estimated from the former (e.g. Zoback 2007, p. 113-116; Mavko et al. 2009, p. 386-388). The empirical correlations are intended to represent the average behaviour of a wide range of lithologies, and so their usefulness is limited by how sensitive the correlated property is to the differences in lithology encountered in the region of interest as well as to any other variable that has not been accommodated within the fitted equation. Nevertheless, albeit with this caveat, such correlations are being used to develop increasingly sophisticated geomechanical models, particularly when more comprehensive input data, such as pre-stack depth migrated (PSDM) seismic inversion, S-wave velocities and borehole information, is also available to provide additional constraints (e.g. White et al. 2007; Sengupta et al. 2011; Gray et al. 2012).

In this study, we have only a very restricted dataset (primarily P-wave). The unavailability of more comprehensive datasets imposes limits on the extent to which we can validate our model results. However the results can be viewed as representative for the context and methodology can be readily applied and tested for more sophisticated dataset in the Caspian and beyond.

and so our comments in this respect are based on whether or not the model results seem realistic given the geomechanical context of the ACG.

The empirical correlations used to infer physical properties and stress states are listed in Table 1. Gradients of overburden, pore fluid pressure and fracture pressure have been evaluated as the change of magnitude of the given quantity over given change in depth.

Given the limited dataset, elastic rock properties were approximated as isotropic throughout the study. The matrix density (ρ_{matrix} = 2600 kg/m^3) in Table 1, Eq. 3 was approximated assuming that the rock is an aggregate of clay minerals comprising 32.5% montmorillonite, 43.5% illite, 17.5% kaolinite, 6.5% chlorite, which is applicable for the Northwest SCB at a depth range of 1-2 km (Buryakovsky et al. 1995). Pore fluid density (ρ_{fluid}) was approximated as 1000 kg/m^3 (Tozer & Borthwick 2010). The horizontal stress formula (Table 1, Eq. 11) makes the commonly used approximation of zero horizontal strain (no lateral expansion) which, together with material isotropy, means that the local horizontal stresses are approximated as the same in all directions.

Fracture pressure (Table 1, Eq. 14) represents the pressure in the borehole that is needed to cause fracturing of the formation. Assuming zero tensile strength, fracture pressure is given by the minimum horizontal stress.

In an attempt to put bounds on the real variation in horizontal stress, the approach of using stress polygons that was introduced by Zoback et al. (1986) and Moos et al. (1990) has been implemented. Stress polygons show permissible ranges of horizontal stresses at a given depth for given pore fluid pressure for each of the three Andersonian fault regimes (Fig. 4). Upper and lower bounds of maximum and minimum horizontal stresses on the stress polygons are constrained by the following relationships derived from the Coulomb failure criterion assuming that one of the principal stresses is vertical (Zoback 2007):

Normal fault
$$\frac{\sigma_v - P_p}{\sigma_h - P_p} \leq \left[\left(\mu^2 + 1\right)^{1/2} + \mu \right]^2 \quad (1)$$

Strike-slip fault
$$\frac{\sigma_H - P_p}{\sigma_h - P_p} \leq \left[\left(\mu^2 + 1\right)^{1/2} + \mu \right]^2 \quad (2)$$

Reverse fault
$$\frac{\sigma_H - P_p}{\sigma_v - P_p} \leq \left[\left(\mu^2 + 1\right)^{1/2} + \mu \right]^2 \quad (3)$$

where σ_v is the vertical principal stress, σ_H is the maximum horizontal principal stress, σ_h is the minimum horizontal principal stress, P_p is the pore fluid pressure and μ is the coefficient of friction. The diagonal line ($\sigma_H = \sigma_h$) in the diagram is intersected by vertical and horizontal lines which constrain the stress ranges for the different fault regimes. Stress polygons are always above the diagonal line because $\sigma_H \geq \sigma_h$.

In regions of excess pore pressure (overpressure) differences between the magnitudes of the principal stresses are small and therefore small stress perturbations can lead to a change from one fault regime to another (Zoback 2007).

Feasibility calculations

In order to establish that the equations listed in Table 1 return realistic values of material properties and stresses within a South Caspian Basin context, we have evaluated these properties and stresses on an SCB mud volcano for which a structural model exists in the public domain. This is located within the Kurdashi-Araz-Deniz (KAD) anticlinal structure on the western margin of the SCB at a water depth of 30-770 m. The calculations were performed for depths of 500m and 1500m below sea floor. These were selected from a seismic section across the mud volcano (Soto et al. 2011) to represent points on the structural crest and flank of the mud volcano respectively (Fig. 5).

Hamilton (1979) established a generalized relationship between acoustic wave velocities and depth in marine sediments. This relationship was used to obtain the P- and S-wave values for the crest and flank locations (Fig. 6).

The SCB is characterized by abnormally high formation pressures and consequently there have been several studies that have attempted to characterize shale compaction within the basin. The porosity-depth curve compiled by Bredehoeft et al. (1988) (Fig. 7) was used to obtain porosity values for the calculations.

Hence the input parameters for the calculations are as listed in Table 2.

Using these input parameters and the equations listed in Table 1, the material properties and stresses listed in Table 3 for the crest and flank of the mud volcano were obtained. These are compared in Table 3 with typical ranges of these values for the material properties of clay minerals and poorly consolidated sandstones and mudstones, and with the stress states previously reported in the South Caspian Basin.

Our calculated values are consistent with those reported in the literature, and so we have confidence that the empirical correlations detailed in Table 1 are not significantly affected by local factors specific to the South Caspian Basin.

2D model

Input parameters and procedure

The mechanical properties and stresses on a 2D vertical section across an ACG mud volcano were modelled by digitizing the P-wave velocities presented on a Full Waveform Inversion (FWI) image published by Selwood et al. (2013). The seismic line was 10 km long by 5 km deep, in an unknown orientation across one of the mud volcanoes in the Azeri part of the ACG field.

The digitization process involved:

1. importing the image into MATLAB®;
2. reading Red (R), Green (G) and Blue (B) values and replacing these RGB triplets with a single value per pixel;
3. replacing each pixel value with the corresponding velocity obtained from the colour bar key to the image;
4. generating the 2D synthetic seismic line and writing it as a SEG-Y file;
5. importing the SEG-Y file into PETREL® for calculations and visualisation.

The resulting P-wave velocity section is shown in Fig. 8. Values of density, porosity and mechanical properties (elastic properties and strength), together with the magnitudes of the principal stresses, pore fluid and fracture pressures were calculated from the P-wave velocities using the equations listed in Table 1 within the PETREL® software package and are presented here as sections showing the 2D variation of these values. In addition, a vertical pseudo-well (RM-1) located on the structural crest was incorporated into the 2D model to assess the modelled parameters in 1D along the well trajectory. The calculations were performed for an average water depth of 120m, which is the average water depth in the Azeri field given by the bathymetry data of Hill et al. (2015).

Results

Since the physical properties were calculated solely from P-wave velocity information, the spatial variation of these properties matches that of the P-wave velocity data (Fig. 8). The empirical correlations listed in Table 1 do, however, provide the magnitudes of the material properties and how these magnitudes vary across the mud volcano in the study area. The variation in elastic properties along the pseudo-well is illustrated in Fig. 9. The values of these elastic properties at a depth of 500 m below sea floor are similar to those obtained at this depth on the structural crest of the KAD mud volcano.

Bulk density values were estimated using Quijada & Stewart's method (Table 1. Eq. 2). Quijada & Stewart (2007) have suggested that in their equation different values of the constants, a and m, are applicable for sands (a=224.9 and m=0.2847) and for shales (a=516.2 and m=0.1896). In this study the lithology was assumed to be an aggregate of clay minerals, and hence the coefficients for shales were used. Fig. 10 shows the variation of bulk density across the 2D section and along the pseudo-well. The values of bulk density are consistent with the bulk density values calculated at the corresponding positions on the KAD mud volcano. Within the vicinity of the mud volcano feeder system relatively small bulk densities persist to greater depths, presumably because the lithologies are in a brecciated and/or fluidised state.

Theoretical and inferred porosity ($□_t$ and □, respectively) values were computed along the crestal pseudo-well RM-1 using Table 1, Eqs. 3 and 4 (Fig. 11). The theoretical porosity curve assumes a normal compaction trend. The 'pressure transition zone' defined as the depth interval between when the inferred porosity curve starts to deviate from the theoretical porosity profile and when the rate of decrease of inferred porosity with depth significantly decreases (Swarbrick & Osborne 1996), lies between 620 metres below sea floor (mbsf) and 2600 mbsf at the crestal pseudo-well RM-1.

Values of pore fluid pressure and fracture pressure have been calculated along the pseudo-well RM-1 (Fig. 12). Estimated pore fluid pressures over the depth range 2-5 km are about 1.4-1.8 times hydrostatic pressure in agreement with previous estimates of shale pore fluid pressure within the South Caspian Basin (Bredehoeft et al. 1988; Javanshir et al. 2015). On the 2D section relatively small pore fluid pressures are seen to persist to a depth of 620 mbsf in areas close to the mud volcano (Fig. 13), and these perhaps represent areas that have not yet fully recharged following recent eruptions.

The friction angle increases with depth but with anomalously small values in the volcano vent area (Fig. 14), perhaps reflecting the relatively unconsolidated state of the sediments in this area. At depths greater than ~2500 m, the friction angle values are in good agreement with the frictional properties given by Byerlee's law (Schön 2011).

Discussion

Fluid flow

The spatial variation of fluid overpressure provides information about the direction of fluid flow near the mud volcano. In Fig. 15 fluid overpressure is plotted as overpressure abnormality factor, which is defined as the ratio of pore fluid pressure to hydrostatic pressure. The study area reveals an abnormality factor of ~1.2 in the first 620 mbsf, ~1.5 in the depth range of 620-2600 mbsf and ~1.8 from 2600 up to 5000 mbsf. As well as decreasing upwards, fluid overpressure decreases from the flanks towards the structural crest of the mud volcano, implying that a component of the regional fluid flow is being directed laterally from the flanks to the crest. These observations support the suggestion that the perceived drive for the mud volcanoes in the offshore South Caspian Basin involves lateral as well as upward pressure transfer. They also point to the possibility of using P-wave data, particularly if supported with direct fluid pressure measurements, to assess fluid flow pathways within the stratigraphy.

Contemporary stress regime

The orientation of the present day stress field is commonly assessed using earthquake focal mechanism solutions and borehole stress orientation measurements. However, it has also been noted that when $\sigma_H \neq \sigma_h$ mud volcano calderas have a tendency to be elliptical with the long axis oriented parallel to σ_h (Bonini 2012). While analysing the bathymetry image from the Azeri side of the ACG field (Hill et al. 2015), we have observed that both mud volcano calderas present in the region of interest are elliptical (Fig. 16a). In each case, the long axis of the caldera is oriented NW-SE, parallel to the orientation of Absheron-Balkhan uplift zone, while the short axis is oriented NE-SW. This implies that σ_h is oriented NW-SE and σ_H is oriented NE-SW. This is consistent with focal mechanism studies performed over the basin (Ritz et al. 2006; Jackson et al. 2012), with borehole breakout data in the World Stress Map database (Heidbach et al. 2008), and with the direction of maximum regional compressive stress inferred from the NE-SW directed subduction of the South Caspian basement beneath the Absheron-Balkhan uplift (Fig. 16b).

An analysis using stress polygons provides further constraints on the stress state. These have been calculated at three different depths along the pseudo-well RM-1 using Eqs. 1-3. So that the three stress polygons can be compared on a single plot, following Zoback (2007) the stresses obtained using Eqs. 1-3 have been normalized by the depth at which each was obtained and so are presented as MPa/m. The input values of vertical stress, pore fluid pressure and coefficient of friction are those at the given depth in the pseudo-well RM-1, while the minimum and maximum horizontal stress values have been obtained by manipulating Eqs. 1 and 3, respectively. The values obtained are listed in Table 4, and the resulting stress polygons are shown in Fig. 17. We find that the stress polygons shrink with increasing depth, as overpressure increases. This finding is consistent with the notion that the principal stresses tend to become closer to the vertical stress in magnitude with increasing depth in overpressured areas, and hence that relatively small changes in the stress field can lead to a shift from one Andersonian fault regime to another (Zoback 2007).

Implications on drillability

Pore fluid pressure and fracture pressure, together with their corresponding depth gradients, are central considerations when establishing safe drilling strategies. Whilst knowledge of the actual magnitudes of these pressures is important for drilling activities, knowledge of their gradients is more practical, as the required drilling mud weight is estimated in pressure gradients. The pore pressure gradient characterizes the minimum (or the lower bound) mud weight and the fracture gradient indicates the maximum (or the upper bound) mud weight (Eaton 1969). Identifying upper and lower bounds on the fracture gradient itself is generally good practice when using estimates of fracture gradient. The lower bound is defined as the fracture closure pressure, which is best measured by a leak-off test, while the upper bound indicates a point at which mud loss from the borehole to induced fractures occurs (Zhang 2011). Estimating these bounds requires knowledge of the magnitudes of the horizontal stresses, the tensile strength, and the thermal stress induced by the difference between the mud and formation temperatures. Since we do not have these parameters, we have used a method by Mathews & Kelly (1967) (Table 1, Eq. 14) to determine fracture pressure and its gradient. This method provides a value similar to the lower bound on the fracture gradient. Fig. 18 shows the pressures and gradients estimated for the crestal pseudo-well RM-1. The large fluctuations in the pore fluid pressure gradient at shallow depths (>500 mbsf) are probably artefacts arising from the resolution of the P-wave velocity and how this impacts on the calculated porosity used to estimate pore fluid pressure (Table 1, Eq. 13). However, the changes in the slope of the depth variation of pore fluid and fracture gradient that occurs at 620 and 2600 mbsf correlate with the top and base of pressure transition zone identified in Fig. 11.

We have attempted to define the safe drilling window (where drilling window is defined as the difference between the fracture gradient and the pore fluid pressure gradient) using our results (Fig. 19). We observe that above a depth of ~300 mbsf, on one flank of the mud volcano the drilling window gradients are as small as ~0.003 MPa/m, whereas on the other flank the gradients are larger (up to 0.012 MPa/m). The model identifies some areas with large drilling window gradients that are close to the mud volcano feeder pipe. These may represent zones of fluid recharging and so may be transient features. Fluid venting pipes are known to extend down to around 2 km beneath the seabed in the ACG (Javanshir et al. 2015), which almost marks the base of pressure transition zone (2600 mbsf) in this study. The areas below the pressure transition zone are characterized by the drilling window gradients of 0.004 MPa/m, which decrease to 0.002 MPa/m with increasing depth. We interpret these values as estimates of the drilling window for deep overpressured sections where well consolidated sediments reside.

Limitations of this study

Key sources of data for full geomechanical modelling include seismic and borehole data, while geological and drilling data are used for calibration purposes. Geological and seismic data provide regional scale information for the entire section (overburden, underburden and zone of interest), whereas drilling and borehole data aid in focusing on a zone of interest with greater accuracy and higher resolution.

The analysis in this study is built almost entirely on P-wave velocity and therefore is sensitive to how tightly constrained the empirical correlations between P-wave velocity and the various mechanical properties and stresses are. A key limitation imposed by the nature of the data is the lack of opportunity to incorporate mechanical anisotropy. Given that the most significant causes of mechanical anisotropy are (a) oriented fractures, (b) textural alignment of highly anisotropic minerals, and (c) compositional banding, one can expect that the mechanical properties of a fractured, well-bedded, clay mineral rich sequence will be anisotropic. Hence considerable confidence could be added to the findings presented here if data that allowed mechanical anisotropy to be quantified (e.g., AVO, VSP, multi-, wide-, rich and full-azimuth seismic) were available. Nevertheless, even with the limited data available, the findings are consistent with the geodynamic context of this part of the South Caspian Basin.

Conclusions

A 2D P-wave velocity dataset was used with empirical correlations between P-wave and various mechanical properties to build a geomechanical model of the area around a mud volcano in the South Caspian Basin. The key findings are:

- realistic values of elastic and brittle strength properties together with fluid pressures can be obtained using the empirical correlations;
- sections showing the spatial variation of pore fluid overpressure around the mud volcanoes calculated from P-wave velocity data have considerable potential for constraining models of fluid flow around these structures;
- preliminary estimates based on seismic velocities provide useful reconnaissance indications of regions that are safe to drill, regions that are risky, and regions that should be avoided.

Taken together, these findings help to reinforce the observation that a considerable body of geomechanical information can be recovered even from very limited seismic datasets, and that this can be useful both for defining targets for more comprehensive geomechanical studies and for providing guidance on drilling strategies.

Acknowledgements

This work was funded by the Ministry of Education of Republic of Azerbaijan. The authors would like to thank Peter Cook from BP Exploration (Caspian Sea) Limited, for the discussions that helped shape the preliminary concepts of the feasibility study. We gratefully acknowledge the comments of Ravan Gulmammadov on an earlier version of the manuscript and Andrew M.W. Newton for his assistance on extracting and processing the bathymetric map of the study area. We would also like to acknowledge the use of SeisLab, which is a set of MATLAB codes for reading and writing standard SEG-Y files that has been placed in the public domain by Eike Rietsch. David Iacopini and an anonymous reviewer are thanked for their constructive feedback. We thank Schlumberger for the provision of Petrel.

References

ABRAMS, M.A. & NARIMANOV, A.A. 1997. Geochemical evaluation of hydrocarbons and their potential sources in the western South Caspian depression, Republic of Azerbaijan. *Marine and Petroleum Geology Petroleum Geology*, **14**, 451–468, doi: 10.1016/S0264-8172(97)00011-1.

ALLEN, P.A. & ALLEN, J.R. 2013. *Basin Analysis: Principles and Application to Petroleum Play Assessment*, 3rd ed. Wiley-Blackwell.

AVSETH, P., MUKERJI, T. & MAVKO, G. 2010. *Quantitative Seismic Interpretation: Applying Rock Physics to Reduce Interpretation Risk*, 1st ed. Cambridge University Press.

AZZARO, E., BELLANCA, A. & NERI, R. 1993. Mineralogy and geochemistry of Mesozoic black shales and interbedded carbonates, southeastern Sicily: Evaluation of diagenetic processes. *Geological Magazine*, **130**, 191–202, doi: 10.1017/S0016756800009857.

BONINI, M. 2008. Elliptical mud volcano caldera as stress indicator in an active compressional setting (Nirano, Pede-Apennine margin, northern Italy). *Geology*, **36**, 131–134, doi: 10.1130/G24158A.1.

BONINI, M. 2012. Mud volcanoes: Indicators of stress orientation and tectonic controls. *Earth-Science Reviews*, **115**, 121–152, doi: 10.1016/j.earscirev.2012.09.002.

BONINI, M. 2013. Fluid seepage variability across the external Northern Apennines (Italy): Structural controls with seismotectonic and geodynamic implications. *Tectonophysics*, **590**, 151–174, doi: 10.1016/j.tecto.2013.01.020.

BREDEHOEFT, J.D., DJEVANSHIR, R.D. & BELITZ, K.R. 1988. Lateral fluid flow in a compacting sand-shale sequence: South Caspian Basin. *AAPG Bulletin*, **72**, 416–424, doi: 10.1306/703C9A1E-1707-11D7-8645000102C1865D.

Bristow, C.R., Gale, I.N., Fellman, E., Cox, B.M., Wilkinson, I.P. & Riding, J.B. 2000. The lithostratigraphy, biostratigraphy and hydrogeological significance of the mud springs at Templars Firs, Wootton Bassett, Wiltshire. *Proceedings of the Geologists' Association*, **111**, 231–245, doi: 10.1016/S0016-7878(00)80016-4.

Buryakovsky, L. A., Chilingar, G. V. & Aminzadeh, F. 2001. *Petroleum Geology of the South Caspian Basin*, 1st ed. Elsevier, doi: 10.1016/B978-088415342-9/50000-X.

Buryakovsky, L.A., Djevanshir, R.D. & Chilingar, G. V. 1995. Abnormally-high formation pressures in Azerbaijan & the South Caspian Basin (as related to smectite ⍰ illite transformations during diagenesis & catagenesis). *Journal of Petroleum Science and Engineering*, **13**, 203–218, doi: 10.1016/0920-4105(95)00008-6.

Byerlee, J. 1978. Friction of rocks. *Pure and Applied Geophysics*, **116**, 615–626, doi: 10.1007/BF00876528.

Calvès, G., Huuse, M., Schwab, A. & Clift, P. 2008. Three-dimensional seismic analysis of high-amplitude anomalies in the shallow subsurface of the northern Indus Fan: Sedimentary and/or fluid origin. *Journal of Geophysical Research*, **113**, 1–16, doi: 10.1029/2008JB005666.

Carragher, P.D., Ross, A., Roach, E., Trefry, C., Talukder, A. & Stalvies, C. 2013. Natural seepage systems at Biloxi & Dauphin domes and Mars mud volcano, north east Mississippi Canyon protraction area, Gulf of Mexico. *Offshore Technology Conference*, 1–19.

Cartwright, J., Huuse, M. & Aplin, A. 2007. Seal bypass systems. *AAPG Bulletin*, **91**, 1141–1166, doi: 10.1306/04090705181.

Castagna, J.P., Batzle, M.L. & Eastwood, R.L. 1985. Relationships between compressional-wave in elastic silicate rocks and shear-wave velocities. *Geophysics*, **50**, 571–581, doi: 10.1190/1.1441933.

Chang, C., Zoback, M.D. & Khaksar, A. 2006. Empirical relations between rock strength and physical properties in sedimentary rocks. *Journal of Petroleum Science and Engineering*, **51**, 223–237, doi: 10.1016/j.petrol.2006.01.003.

CLARKE, R.H. & CLEVERLY, R.W. 1991. Petroleum seepage and post-accumulation migration. *Geological Society of London, Special Publications*, **59**, 265–271, doi: 10.1144/GSL.SP.1991.059.01.17.

CONTET, J. & UNTERSEH, S. 2015. Multiscale site investigation of a giant mud-volcano offshore Azerbaijan - Impact on subsea field development. *Offshore Technology Conference*, **OTC-25864**, 1–10, doi: 10.4043/25864-MS.

DAVIES, R.J. & STEWART, S.A. 2005. Emplacement of giant mud volcanoes in the South Caspian Basin: 3D seismic reflection imaging of their root zones. *Journal of the Geological Society*, **162**, 1–4, doi: 10.1144/0016-764904-082.

DEVILLE, E., BATTANI, A., ET AL. 2003. The origin and processes of mud volcanism: New insights from Trinidad. *Geological Society of London, Special Publications*, **216**, 475–490, doi: 10.1144/GSL.SP.2003.216.01.31.

DIMITROV, L.I. 2002. Mud volcanoes - The most important pathway for degassing deeply buried sediments. *Earth-Science Reviews*, **59**, 49–76, doi: 10.1016/S0012-8252(02)00069-7.

EATON, B. 1969. Fracture gradient prediction and its application in oilfield operations. *Journal of Petroleum Technology*, **21**, 1353–1360, doi: 10.2118/2163-PA.

EVANS, R., DAVIES, R. & STEWART, S. 2006. Mud volcano evolution from 3D seismic interpretation and field mapping in Azerbaijan. *In*: *AAPG/GSTT Hedberg Conference: Mobile Shale Basins - Genesis, Evolution & Hydrocarbon Systems Abstracts*.

EVANS, R.J., DAVIES, R.J. & STEWART, S.A. 2007. Internal structure and eruptive history of a kilometre-scale mud volcano system, South Caspian Sea. *Basin Research*, **19**, 153–163, doi: 10.1111/j.1365-2117.2007.00315.x.

EVANS, R.J., STEWART, S.A. & DAVIES, R.J. 2008. The structure and formation of mud volcano summit calderas. *Journal of the Geological Society*, **165**, 769–780, doi: 10.1144/0016-76492007-118.

Feseker, T., Brown, K.R., et al. 2010. Active mud volcanoes on the upper slope of the western Nile Deep-sea fan - First results from the P362/2 cruise of R/V poseidon. *Geo-Marine Letters*, **30**, 169–186, doi: 10.1007/s00367-010-0192-0.

Feyzullayev, A.A. 2012. Mud volcanoes in the South Caspian Basin: Nature and estimated depth of its products. *Natural Science*, **04**, 445–453, doi: 10.4236/ns.2012.47060.

Feyzullayev, A.A. & Lerche, I. 2009. Occurrence and nature of overpressure in the sedimentary section of the South Caspian Basin, Azerbaijan. *Energy Exploration & Exploitation*, **27**, 345–366.

Feyzullayev, A.A. & Movsumova, U.A. 2010. The nature of the isotopically heavy carbon of carbon dioxide and bicarbonates in the waters of mud volcanoes in Azerbaijan. *Geochemistry International*, **48**, 517–522, doi: 10.1134/S0016702910050083.

Fjaer, E., Holt, R.M., Horsrud, P., Raaen, A.M. & Risnes, R. 2008. *Petroleum Related Rock Mechanics*, 2nd ed. Elsevier, doi: 10.1016/0148-9062(93)92632-Z.

Foster, D., Fowler, S., McGarrity, J., Riviere, M., Robinson, N., Seaborne, R. & Watson, P. 2008. Building on BP's large-scale OBC monitoring experience - The Clair and Chirag-Azeri Projects. *Society of Exploration Geophysicists*, **27**, 1632–1637, doi: 10.1190/1.3036967.

Gardner, G.H.F., Gardner, L.W. & Gregory, A.R. 1974. Formation velocity and density - The diagnostic basis of stratigraphic traps. *Geophysics*, **39**, 770–780, doi: 10.1190/1.1440465.

Gray, D., Anderson, P., Logel, J., Delbecq, F., Schmidt, D. & Schmid, R. 2012. Estimation of stress and geomechanical properties using 3D seismic data. *First Break*, **30**, 59–68.

Guliyev, I., Aliyeva, E., Huseynov, D., Feyzullayev, A. & Mamedov, P. 2010. Hydrocarbon potential of ultra deep deposits in the South Caspian Basin (presentation). *AAPG European Region Annual Conference*, 1–66, doi: http://www.searchanddiscovery.com/documents/2011/10312guliyev/ndx_guliyev.pdf.

Guliyev, I.S., Feizulayev, A.A. & Huseynov, D.A. 2001. Isotope geochemistry of oils from fields and mud volcanoes in the South Caspian Basin, Azerbaijan. *Petroleum Geoscience*, **7**, 201–209, doi: 10.1144/petgeo.7.2.201.

Hamilton, E.L. 1979. Vp/Vs & Poisson's ratios in marine sediments and rocks. *Acoustical Society of America*, **66**, 1093–1101, doi: 10.1121/1.383344.

Heidbach, O., Tingay, M., Barth, A., Reinecker, J., Kurfeß, D. & Müller, B. 2008. The World Stress Map database release 2008 doi:10.1594/GFZ.WSM.Rel2008.

Hill, A.W., Hampson, K.M., Hill, A.J., Golightly, C., Wood, G.A., Sweeney, M. & Smith, M.M. 2015. ACG field geohazards management: Unwinding the past, securing the future. *Offshore Technology Conference*, **OTC-25870**, 1–22, doi: 10.4043/25870-MS.

Hong, W.L., Etiope, G., Yang, T.F. & Chang, P.Y. 2013. Methane flux from miniseepage in mud volcanoes of SW Taiwan: Comparison with the data from Italy, Romania and Azerbaijan. *Journal of Asian Earth Sciences*, **65**, 3–12, doi: 10.1016/j.jseaes.2012.02.005.

Horsrud, P. 2001. Estimating mechanical properties of shale from empirical correlations. *SPE Drilling & Completion*, **16**, 68–73, doi: 10.2118/56017-PA.

Hovland, M., Hill, A. & Stokes, D. 1997. The structure and geomorphology of the Dashgil mud volcano, Azerbaijan. *Geomorphology*, **21**, 1–15, doi: 10.1016/S0169-555X(97)00034-2.

Hubbert, K.M. & Rubey, W.W. 1959. Role of fluid pressure in mechanics of overthrust faulting. Part I. Mechanics of fluid-filled porous solids and its application to overthrust faulting. *Geological Society of America Bulletin*, **70**, 115–166, doi: 10.1130/0016-7606(1959)70[167:ROFPIM]2.0.CO;2.

Islam, M.A. & Skalle, P. 2013. An experimental investigation of shale mechanical properties through drained and undrained test mechanisms. *Rock Mechanics and Rock Engineering*, **46**, 1391–1413, doi: 10.1007/s00603-013-0377-8.

Iverson, W.P. 1995. Closure stress calculations in anisotropic formations. *Society of Petroleum Engineers*, 535–548, doi: 10.2118/29598-MS.

JACKSON, J., PRIESTLEY, K., ALLEN, M. & BERBERIAN, M. 2002. Active tectonics of the South Caspian Basin. *Geophysical Journal International*, **148**, 214–245, doi: 10.1046/j.1365-246X.2002.01005.x.

JAEGER, J.C., COOK, N.G.W. & ZIMMERMAN, R.W. 2007. *Fundamentals of Rock Mechanics*, 4th ed. Blackwell Publishing.

JAVANSHIR, R.J., RILEY, G.W., DUPPENBECKER, S.J. & ABDULLAYEV, N. 2015. Validation of lateral fluid flow in an overpressured sand-shale sequence during development of Azeri-Chirag-Gunashli oil field and Shah Deniz gas field: South Caspian Basin, Azerbaijan. *Marine and Petroleum Geology*, **59**, 593–610, doi: 10.1016/j.marpetgeo.2014.07.019.

JIN, Y., YUAN, J., HOU, B., CHEN, M., LU, Y., LI, S. & ZOU, Z. 2012. Analysis of the vertical borehole stability in anisotropic rock formations. *Journal of Petroleum Exploration and Production Technology*, **2**, 197–207, doi: 10.1007/s13202-012-0033-y.

JONES, R.W. & SIMMONS, M.D. 1997. A review of the stratigraphy of eastern Paratethys (Oligocene-Holocene), with particular emphasis on the Black Sea. *Regional and Petroleum Geology of the Black Sea and Surrounding Region: AAPG Memoir 68*, 39–52.

JUDD, A. 2005. Gas emissions from mud volcanoes: Significance to global climate change. *In*: Martinelli, G. & Panahi, B. (eds) *Mud Volcanoes, Geodynamics & Seismicity*. Springer Netherlands, 147–157., doi: 10.1007/1-4020-3204-8_13.

KOHLI, A.H. & ZOBACK, M.D. 2013. Frictional properties of shale reservoir rocks. *Journal of Geophysical Research: Solid Earth*, **118**, 5109–5125, doi: 10.1002/jgrb.50346.

KOPF, A., STEGMANN, S., DELISLE, G., PANAHI, B., ALIYEV, C.S. & GULIYEV, I. 2009. In-situ cone penetration tests at the sctive Dashgil mud volcano, Azerbaijan: Evidence for excess fluid pPressure, updoming and possible future violent eruption. *Marine and Petroleum Geology*, **26**, 1716–1723, doi: 10.1016/j.marpetgeo.2008.11.005.

Lal, M. 1999. Shale stability: Drilling fluid interaction and shale strength. *SPE Latin America and Caribbean Petroleum Engineering Conference*, 1–10, doi: 10.2118/54356-MS.

Le Pichon, X., Foucher, J.-P., et al. 1990. Mud volcano field seaward of the Barbados accretionary complex: A deep-towed side scan survey. *Journal of Geophysical Research*, **95**, 8917–8929, doi: 10.1029/JB095iB06p08931.

Lerche, I. & Bagirov, E. 1999. *Impact of Natural Hazards on Oil and Gas Extraction - The South Caspian Basin*, 1st ed. Springer US.

Magara, K. 1978. *Compaction and Fluid Migration: Practical Petroleum Geology*, 1st ed. Elsevier.

Mathews, W.R. & Kelly, J. 1967. How to predict formation pressure and fracture gradient. *Oil & Gas Journal*, 7.

Mavko, G., Mukerji, T. & Dvorkin, J. 2009. *The Rock Physics Handbook - Tools for Seismic Analysis of Porous Media*, 2nd ed. Cambridge University Press.

Mazzini, A., Svensen, H., Planke, S., Guliyev, I., Akhmanov, G.G., Fallik, T. & Banks, D. 2009. When mud volcanoes sleep: Insight from seep geochemistry at the Dashgil mud volcano, Azerbaijan. *Marine and Petroleum Geology*, **26**, 1704–1715, doi: 10.1016/j.marpetgeo.2008.11.003.

Milkov, A. V. 2000. Worldwide distribution of submarine mud volcanoes and associated gas hydrates. *Marine Geology*, **167**, 29–42, doi: 10.1016/S0025-3227(00)00022-0.

Moos, D. & Zoback, M.D. 1990. Utilization of observations of well bore failure to constrain the orientation and magnitude of crustal stresses: Application to continental, deep sea drilling project and ocean drilling program boreholes. *Journal of Geophysical Research*, **95**, 9305–9325, doi: 10.1029/JB095iB06p09305.

Morton, A., Allen, M., et al. 2003. Provenance patterns in a neotectonic basin: Pliocene and Quaternary sediment supply to the South Caspian. *Basin Research*, **15**, 321–337, doi: 10.1046/j.1365-2117.2003.00208.x.

Oppo, D., Capozzi, R., Nigarov, A. & Esenov, P. 2014. Mud volcanism and fluid geochemistry in the Cheleken peninsula, western Turkmenistan. *Marine and Petroleum Geology*, **57**, 122–134, doi: 10.1016/j.marpetgeo.2014.05.009.

Pape, T., Feseker, T., Kasten, S., Fischer, D. & Bohrmann, G. 2011. Distribution and abundance of gas hydrates in near-surface deposits of the Håkon Mosby mud volcano, SW Barents Sea. *Geochemistry, Geophysics, Geosystems*, **12**, 1–22, doi: 10.1029/2011GC003575.

Planke, S., Svensen, H., Hovland, M., Banks, D. A. & Jamtveit, B. 2003. Mud and fluid migration in active mud volcanoes in Azerbaijan. *Geo-Marine Letters*, **23**, 258–267, doi: 10.1007/s00367-003-0152-z.

Plumb, R., Edwards, S., Pidcock, G., Lee, D. & Stacey, B. 2000. The mechanical earth model concept and its application to high-risk well construction projects. *IADC/SPE Drilling Conference*, 1–13, doi: 10.2118/59128-MS.

Prasad, M. 2002. Measurement of Young's modulus of clay minerals using atomic force acoustic microscopy. *Geophysical Research Letters*, **29**, 2–5, doi: 10.1029/2001GL014054.

Quijada, M.F. & Stewart, R.R. 2007. Density estimation using density-velocity relations and seismic inversion. *CREWES Research Report*, **19**, 1–20.

Ritz, J.F., Nazari, H., Ghassemi, A., Salamati, R., Shafei, A., Solaymani, S. & Vernant, P. 2006. Active transtension inside central Alborz: A new insight into northern Iran-southern Caspian geodynamics. *Geology*, **34**, 477–480, doi: 10.1130/G22319.1.

Roberts, K.S., Davies, R.J., Stewart, S. A. & Tingay, M. 2011. Structural controls on mud volcano vent distributions: examples from Azerbaijan and Lusi, east Java. *Journal of the Geological Society*, **168**, 1013–1030, doi: 10.1144/0016-76492010-158.

Rubey, W.W. & Hubbert, K.M. 1959. Role of fluid pressure in mechanics of overthrust faulting. Part II. Overthrust belt in geosynclinal area of western Wyoming in light of fluid-pressure hypothesis. *Geological Society of America Bulletin*, **70**, 167–206, doi: 10.1130/0016-7606(1959)70[167:ROFPIM]2.0.CO;2.

SANTOS BETANCOR, I. & SOTO, J.I. 2015. 3D geometry of a shale-cored anticline in the western South Caspian Basin (offshore Azerbaijan). *Marine and Petroleum Geology Petroleum Geology*, **67**, 829–851, doi: 10.1016/j.marpetgeo.2015.06.012.

SCHÖN, J. 2011. *Physical Properties of Rocks: A Workbook*. Elsevier.

SELWOOD, C.S., SHAH, H.M. & BAPTISTE, D. 2013. The evolution of imaging over Azeri, from TTI tomography to anisotropic FWI. *75th EAGE Conference & Exhibition incorporating SPE EUROPEC 2013, Extended abstract*, 1–5.

SENGUPTA, M., DAI, J., VOLTERRANI, S., DUTTA, N., RAO, N.S., AL-QADEERI, B. & KIDAMBI, V.K. 2011. Building a seismic-driven 3D geomechanical model in a deep carbonate reservoir. *SEG Technical Program Expanded Abstracts 2011*, 2069–2073, doi: 10.1190/1.3627616.

SMITH-ROUCH, L.S. 2006. Oligocene-Miocene Maykop/Diatom total petroleum system of the South Caspian Basin province, Azerbaijan, Iran and Turkmenistan. *U.S. Geological Survey Bulletin*, **2201-I**, 1–27.

SOTO, J.I., SANTOS-BETANCOR, I., SANCHEZ BORREGO, I. & MACELLARI, C.E. 2011. Shale diapirism and associated folding history in the South Caspian Basin (Offshore Azerbaijan). *AAPG Annual Convention and Exhibition*, **30162**.

STEWART, S.A. & DAVIES, R.J. 2006. Structure and emplacement of mud volcano systems in the South Caspian Basin. *AAPG Bulletin*, **90**, 771–786, doi: 10.1306/11220505045.

SWARBRICK, R.E. & OSBORNE, M.J. 1996. The nature and diversity of pressure transition zones. *Petroleum Geoscience*, **2**, 111–116, doi: 10.1144/petgeo.2.2.111.

TOZER, R.S.J. & BORTHWICK, A. M. 2010. Variation in fluid contacts in the Azeri field, Azerbaijan: sealing faults or hydrodynamic aquifer? *Geological Society, London, Special Publications*, **347**, 103–112, doi: 10.1144/SP347.8.

UNTERSEH, S. & CONTET, J. 2015. Integrated geohazards assessments offshore Azerbaijan, Caspian Sea. *Offshore Technology Conference*, **OTC-25911**, 1–8, doi: 10.4043/25911-MS.

Vanorio, T., Prasad, M. & Nur, A. 2003. Elastic properties of dry clay mineral aggregates, suspensions and sandstones. *Geophysical Journal International*, **155**, 319–326, doi: 10.1046/j.1365-246X.2003.02046.x.

White, A., Ward, C., Castillo, D., Magee, M., Trotta, J., McIntyre, B. & O'Shea, P. 2007. Updating the geomechanical model and calibrating pore pressure from 3D seismic using data from the Gnu-1 Well, Dampier sub-Basin, Australia. *Proceedings of Asia Pacific Oil and Gas Conference and Exhibition*, 16, doi: 10.2118/110926-MS.

Yusifov, M. & Rabinowitz, P.D. 2004. Classification of mud volcanoes in the South Caspian Basin, offshore Azerbaijan. *Marine and Petroleum Geology*, **21**, 965–975, doi: 10.1016/j.marpetgeo.2004.06.002.

Zang, A., Stephansson, O., Heidbach, O. & Janouschkowetz, S. 2012. World Stress Map database as a resource for rock mechanics and rock engineering. *Geotechnical and Geological Engineering*, **30**, 625–646, doi: 10.1007/s10706-012-9505-6.

Zhang, J. 2011. Pore pressure prediction from well logs: Methods, modifications and new approaches. *Earth-Science Reviews*, **108**, 50–63, doi: 10.1016/j.earscirev.2011.06.001.

Zoback, M.D. 2007. *Reservoir Geomechanics*, 1st ed. Cambridge University Press.

Figure captions

Fig. 1. *(a) Bathymety of the Caspian Sea and topography of the surrounding countries, showing the location of the offshore South Caspian Basin and the Azeri-Chirag-Guneshly (ACG) structure (map extracted using GEBCO_2014 Grid – a global 30 arc-second interval grid – and processed in ArcMap); (b) Simplified tectonic framework for the offshore South Caspian Basin (modified from Stewart & Davies 2006)*

Fig. 2. *Simplified stratigraphic column of the South Caspian Basin. Nomenclature: S – source rock, R – reservoir, C – cap rock (modified from Yusifov & Rabinowitz 2004; Smith-Rouch 2006; Javanshir et al. 2015)*

Fig. 3. *Schematic diagram showing the geometry and key geomechanical properties of the Chirag mud volcano. SSTD – sediment-source top depth, GG – geothermal gradient, PPG – pore-pressure gradient, TH – thickness, Por – porosity, Per – permeability, MCV – mud cone volume, MCT - mud cone thickness, HPE – highest point elevation, SD – surface diameter, WD – water depth, EV – eruption volume, IOD – illitization onset depth, IT – illitization temperature. Superscripts in brackets refer to the references: (1)Evans et al. 2006; (2)Buryakovsky et al. 2001; (3)Stewart & Davies 2006; (4)Evans et al. 2006; (5)Davies et al. 2005; (6)Feyzullayev & Lerche 2009*

Fig. 4. *Stress polygons defining the upper and lower bounds of the principal horizontal stresses in different fault regimes (modified from Zoback, 2007)*

Fig. 5. *Vertical seismic section of a mud volcano from Kurdashi-Araz-Deniz (KAD) structure in the offshore western SCB (modified from Soto et al. 2011)*

Fig. 6. *Generic P- and S-wave velocities vs. depth curves in marine sediments (modified from Hamilton 1979)*

Fig. 7. *Shale compaction curve in northwest SCB (modified from Bredehoeft et al. 1988)*

Fig. 8: *P-wave velocity data generated from the Full Waveform Inversion image published by Selwood et al. (2013). Highlighted is the feeder pipe of the investigated mud volcano*

Fig. 9. *(a) Profiles of elastic rock properties and (b) acoustic wave velocities along the RM-1 pseudo-well. Markers indicate the magnitudes of these properties obtained on the structural crest of the KAD mud volcano that was analysed in the feasibility modelling*

Fig. 10. *(a) Vertical cross-section across the ACG showing the variation in bulk density as obtained using Quijada & Stewart's method with their parameters for shales. (b) The depth variation of bulk density along the pseudo-well RM-1, with the depth variation using Quijada & Stewart's parameters for sands are also shown for comparison*

Fig. 11: *Variation in inferred porosity and theoretical porosity along pseudo-well RM-1 showing the onset of overpressuring at 620 mbsf and the top of 'hard overpressure' at 2600 mbsf*

Fig. 12. *Variation in overburden stress and pressures along pseudo-well RM-1*

Fig. 13: *Vertical cross-section across the ACG showing the variation in pore fluid pressure. This highlights the relatively small pore fluid pressures in the shallow unconsolidated sediments and in the vicinity of the mud volcano*

Fig. 14: *(a) Vertical cross-section across the ACG showing the variation of friction angle and (b) the depth variation of friction angle along the pseudo-well RM-1. The marker on the pseudo-well curve indicates the friction angle obtained on the structural crest of the KAD mud volcano that was analysed in the feasibility modelling*

Fig. 15: *(a) Vertical cross-section across the ACG and (b) along the pseudo-well RM-1 showing the overpressure abnormality factor. Arrows indicate the inferred direction of fluid flow*

Fig. 16: *Regional horizontal stress states in the ACG field. (a) Elliptical mud volcano (MV) calderas drawn on the ACG bathymetry image of Hill et al. (2015). The inset figure is a conceptual diagram of stress states around a mud volcano located in the structural crest of a larger scale antiform (modified from Bonini 2012). On the structural crest, outer arc extension means that the vertical stress is locally probably the greatest principal stress. (b) World Stress Map displaying borehole breakouts from the ACG overlain by a rose diagram of borehole breakout directions; the data are coloured according to confidence in their quality (with A being the highest quality)*

Fig. 17. *Stress polygons at three depths in pseudo-well RM-1, showing the decreasing permissible ranges of horizontal stresses with increasing depth*

Fig. 18: *Variation of pressure gradients along pseudo-well RM-1*

Fig. 19. *Vertical cross-section across the ACG showing the width of the drilling window. The safest areas to drill are those with the widest drilling window*

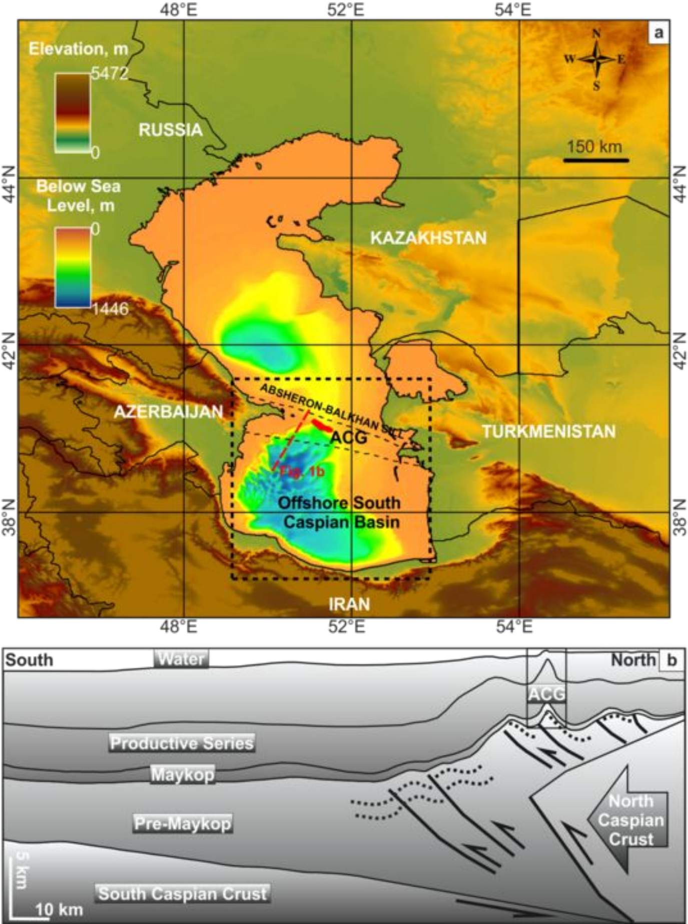
48°E
52°E
54°E
a
Elevation, m
5472
0
RUSSIA
150 km
N
S
W
E
44°N
Below Sea Level, m
0
1446
KAZAKHSTAN
42°N
ABSHERON-BALKHAN SILL
AZERBAIJAN
ACG
TURKMENISTAN
Fig. 1b
Offshore South Caspian Basin
38°N
IRAN
South
Water
North
b
ACG
Productive Series
Maykop
Pre-Maykop
North Caspian Crust
5 km
10 km
South Caspian Crust

Era	Period	Epoch	Formation			Lithology	Average Thickness (m)	Petroleum Potential S	R	C
Cenozoic	Quaternary	Holocene	Recent			Mudstone and siltstone	260-820			
		Pleistocene								
			Absheron				650-1400		●	●
	Neogene	Pliocene	Akchagyl			Shale	30-50	●	●	●
			Productive Series	Upper	Surakhany	Evaporite interbedded with shale	2600-3600			
					Sabunchy	Shale				
					Balakhany	Fluvial sandstone with mudstone intercalations				
					Fasila					
		Miocene		Lower	NKG	Mudstone, siltstone & sandstone	800-1200			
					NKP					
					Kirmaki					
					Pod-Kirmaki					
					Kalin	Marine shale				
			Pontian				10-160			
			Diatom				75-310	●	●	●
			Chokrak				10-50			
			Tarkhan				30			
			Diatom			Organic-rich shale	75-310			
			Maykop				1000	●	●	●
	Palaeogene	Oligocene								
		Eocene				Marine shale	140-250			
		Palaeocene					170-800			
Mesozoic	Cretaceous					Carbonates	>6000	●		
	Jurassic					Volcanics	>4500			

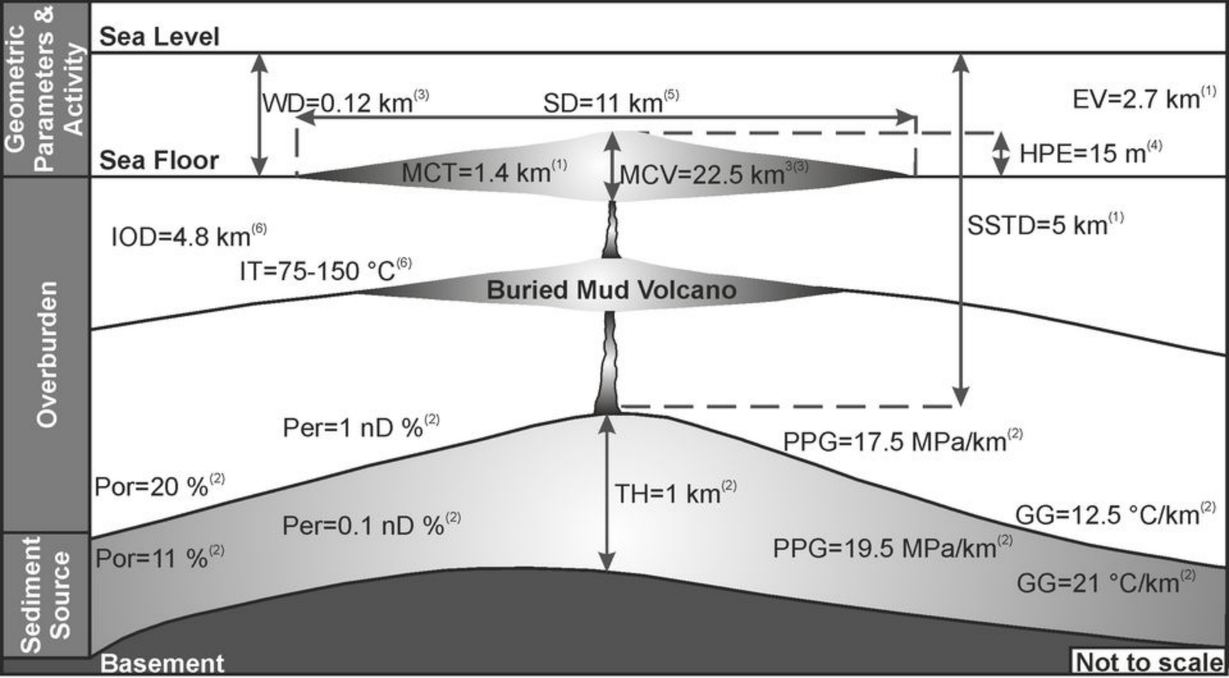

Geometric Parameters & Activity
Sea Level
Sea Floor
WD=0.12 km(3)
SD=11 km(5)
EV=2.7 km(1)
HPE=15 m(4)
MCT=1.4 km(1)
MCV=22.5 km3(3)
SSTD=5 km(1)
Overburden
IOD=4.8 km(6)
IT=75-150 °C(6)
Buried Mud Volcano
Per=1 nD %(2)
PPG=17.5 MPa/km(2)
Por=20 %(2)
TH=1 km(2)
GG=12.5 °C/km(2)
Per=0.1 nD %(2)
PPG=19.5 MPa/km(2)
Sediment Source
Por=11 %(2)
GG=21 °C/km(2)
Basement
Not to scale

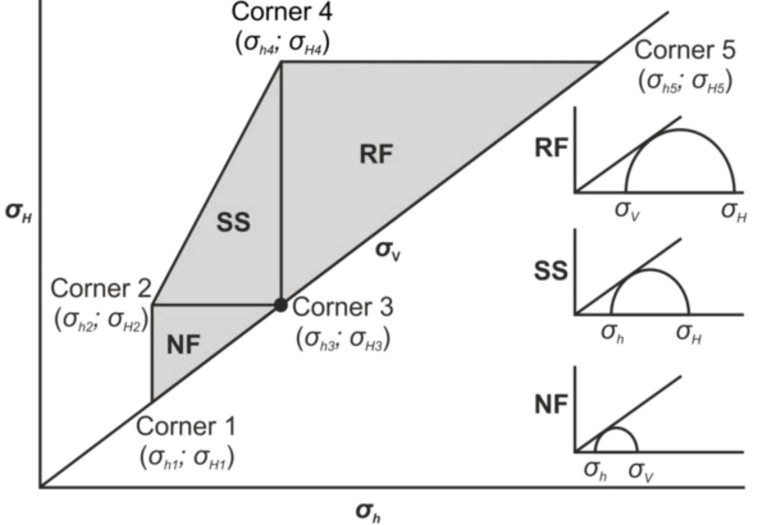

NF - Normal Fault; SS - Strike-slip Fault; RF - Reverse Fault

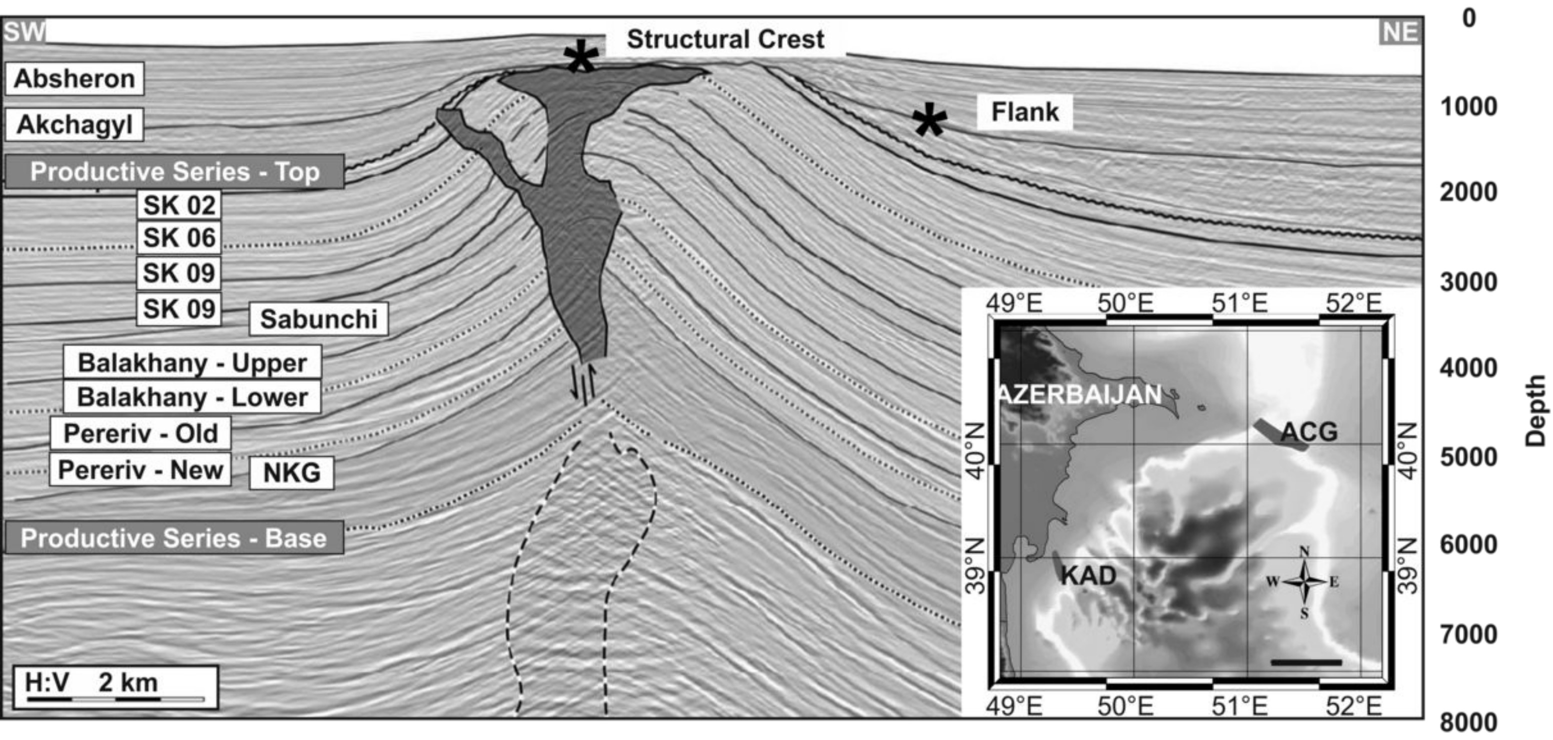

SW
NE
Structural Crest
Absheron
Akchagyl
Flank
Productive Series - Top
SK 02
SK 06
SK 09
SK 09
Sabunchi
Balakhany - Upper
Balakhany - Lower
Pereriv - Old
Pereriv - New
NKG
Productive Series - Base
H:V 2 km
0
1000
2000
3000
4000
5000
6000
7000
8000
Depth
49°E
50°E
51°E
52°E
40°N
39°N
AZERBAIJAN
ACG
KAD
N
S
W
E

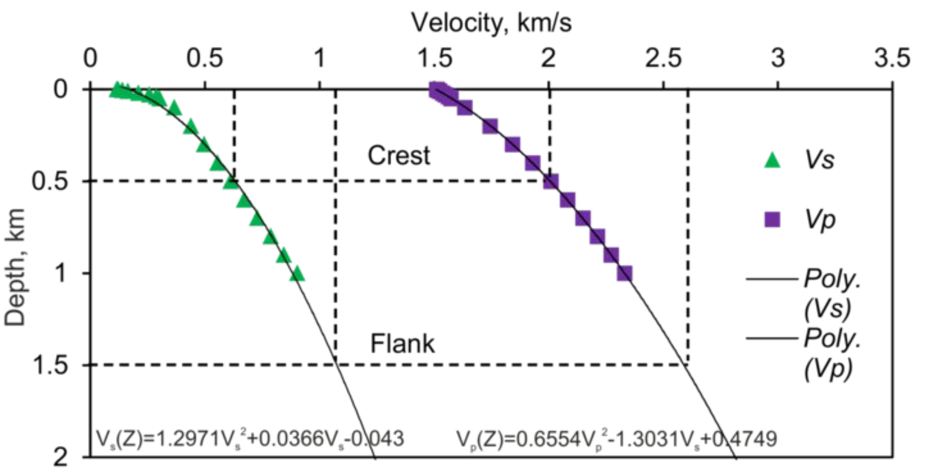

Velocity, km/s
0
0.5
1
1.5
2
2.5
3
3.5
Depth, km
0
0.5
1
1.5
2
Crest
Flank
Vs
Vp
Poly. (Vs)
Poly. (Vp)
Vs(Z)=1.2971Vs2+0.0366Vs-0.043
Vp(Z)=0.6554Vp2-1.3031Vs+0.4749

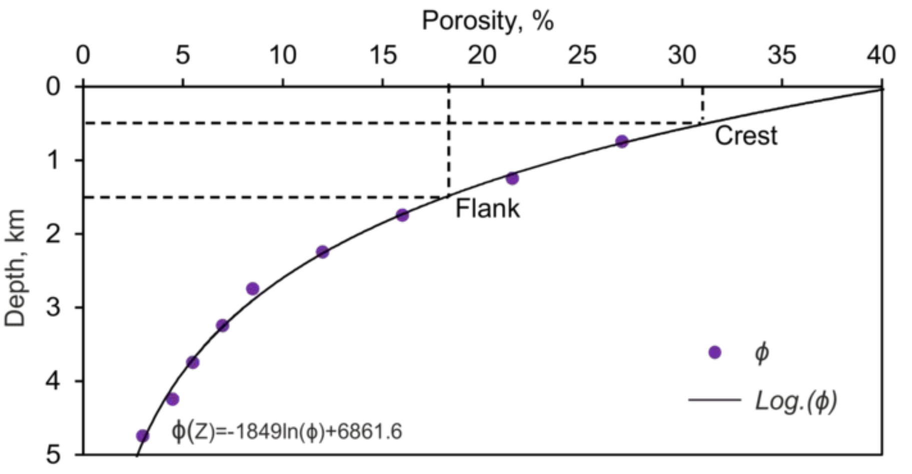

Porosity, %
0
5
10
15
20
25
30
35
40
0
1
2
3
4
5
Depth, km
Crest
Flank
ϕ
Log.(ϕ)
ϕ(Z)=-1849ln(ϕ)+6861.6

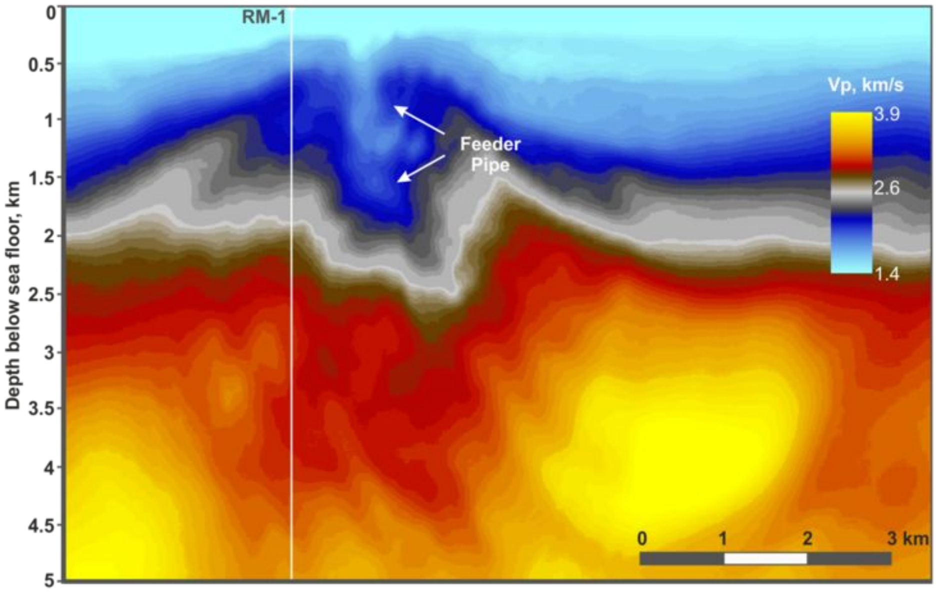

RM-1
Feeder Pipe
Vp, km/s
3.9
2.6
1.4
Depth below sea floor, km
0
0.5
1
1.5
2
2.5
3
3.5
4
4.5
5
0
1
2
3 km

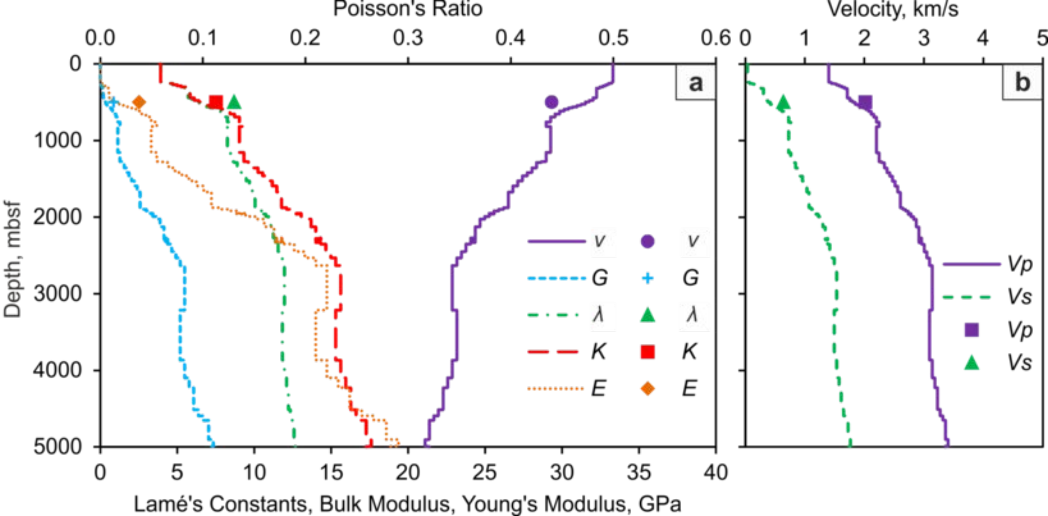

Poisson's Ratio
0.0
0.1
0.2
0.3
0.4
0.5
0.6
Velocity, km/s
0
1
2
3
4
5
0
1000
2000
3000
4000
5000
Depth, mbsf
a
b
v
G
λ
K
E
v
G
λ
K
E
Vp
Vs
Vp
Vs
0
5
10
15
20
25
30
35
40
Lamé's Constants, Bulk Modulus, Young's Modulus, GPa

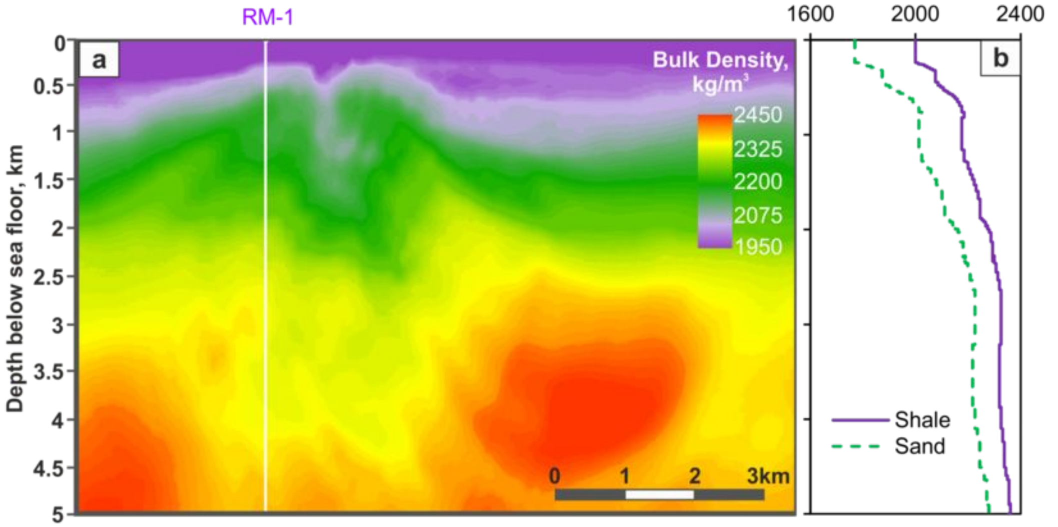

RM-1
a
Bulk Density, kg/m³
2450
2325
2200
2075
1950
0
1
2
3km
Depth below sea floor, km
0
0.5
1
1.5
2
2.5
3
3.5
4
4.5
5
1600
2000
2400
b
Shale
Sand

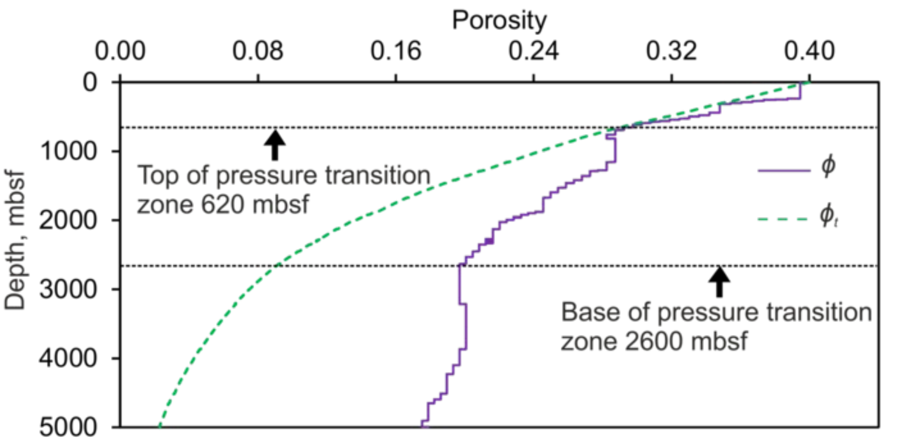

Porosity
0.00
0.08
0.16
0.24
0.32
0.40
0
1000
2000
3000
4000
5000
Depth, mbsf
Top of pressure transition zone 620 mbsf
Base of pressure transition zone 2600 mbsf
ϕ
ϕ_t

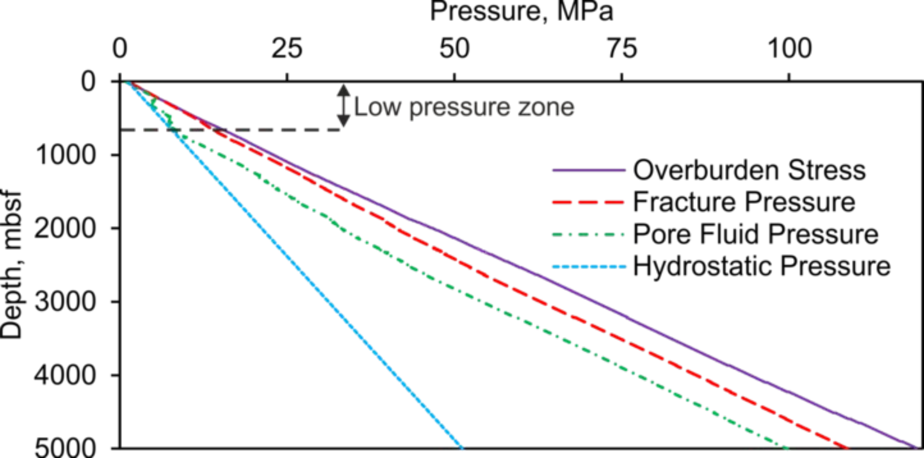
Pressure, MPa
0
25
50
75
100
0
1000
2000
3000
4000
5000
Depth, mbsf
Low pressure zone
Overburden Stress
Fracture Pressure
Pore Fluid Pressure
Hydrostatic Pressure

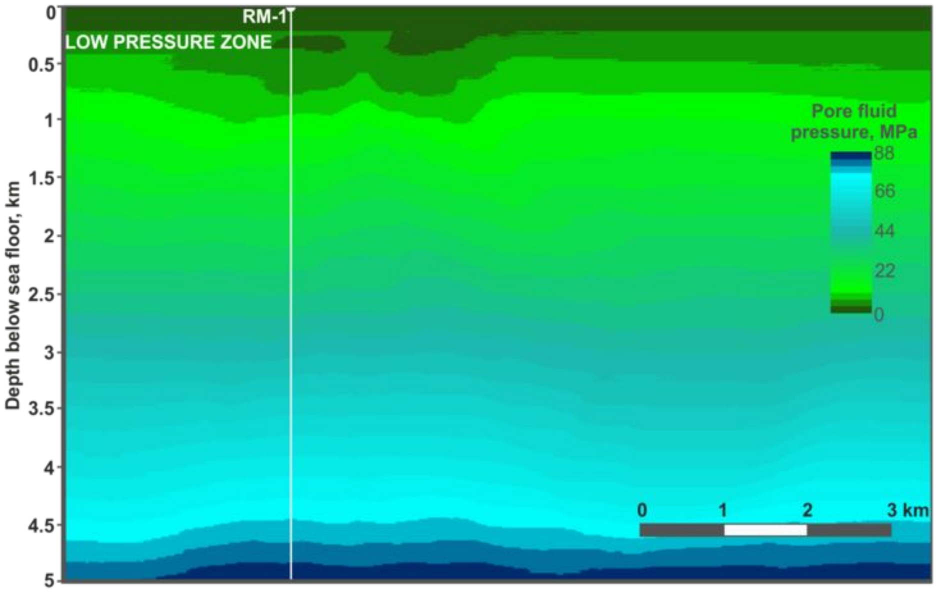
RM-1
LOW PRESSURE ZONE
Depth below sea floor, km
0
0.5
1
1.5
2
2.5
3
3.5
4
4.5
5
Pore fluid pressure, MPa
88
66
44
22
0
0
1
2
3 km

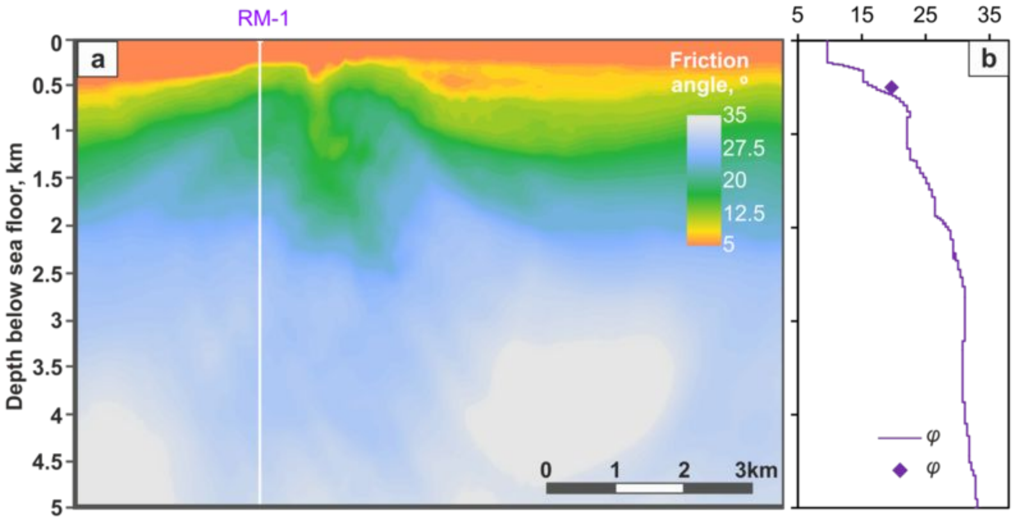

RM-1
a
Friction angle, °
35
27.5
20
12.5
5
Depth below sea floor, km
0
0.5
1
1.5
2
2.5
3
3.5
4
4.5
5
0 1 2 3km
b
5 15 25 35
φ
φ

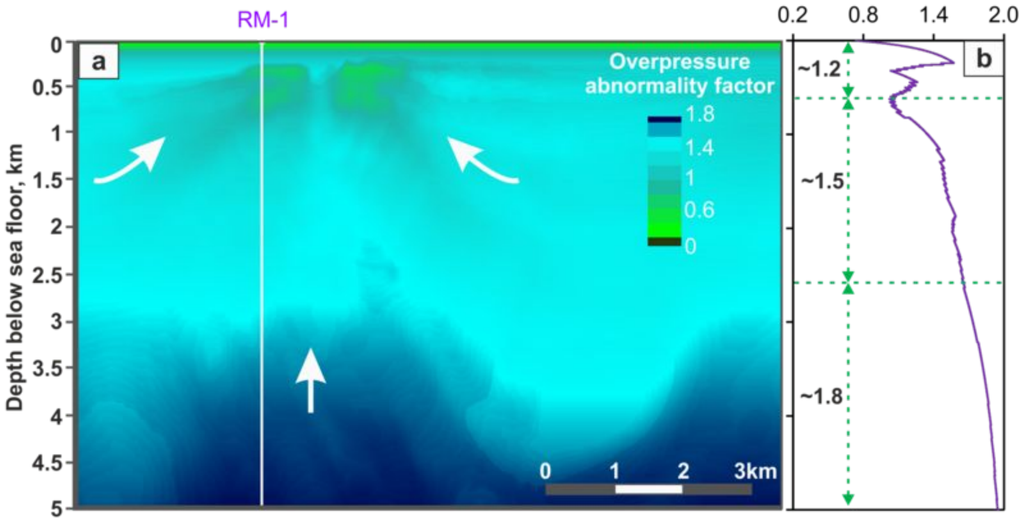
RM-1
a
Overpressure abnormality factor
1.8
1.4
1
0.6
0
Depth below sea floor, km
0
0.5
1
1.5
2
2.5
3
3.5
4
4.5
5
0 1 2 3km
b
0.2 0.8 1.4 2.0
~1.2
~1.5
~1.8

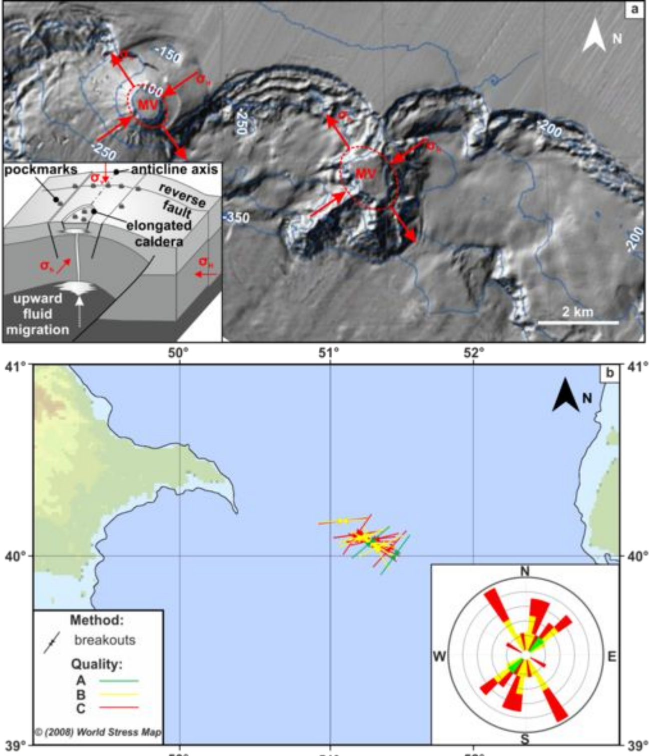
a
N
-150
-100
MV
-250
-250
MV
-200
-350
-200
pockmarks
anticline axis
reverse fault
elongated caldera
upward fluid migration
2 km
50°
51°
52°
41°
40°
39°
b
N
Method:
breakouts
Quality:
A
B
C
© (2008) World Stress Map
W
E
S

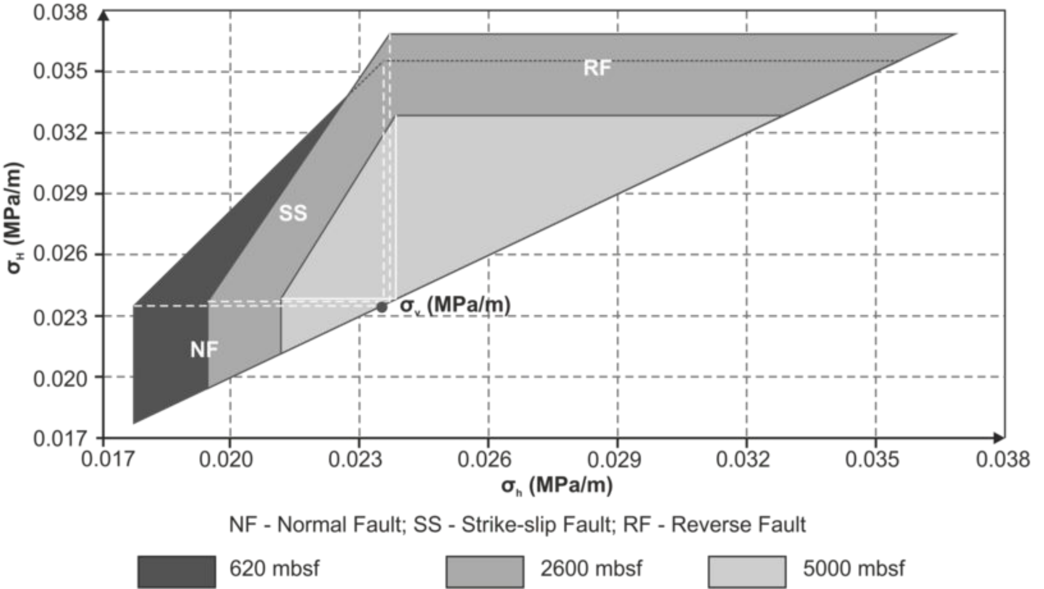

0.038
0.035
0.032
0.029
0.026
0.023
0.020
0.017
σH (MPa/m)
0.017
0.020
0.023
0.026
0.029
0.032
0.035
0.038
σh (MPa/m)
σv (MPa/m)
RF
SS
NF
NF - Normal Fault; SS - Strike-slip Fault; RF - Reverse Fault
620 mbsf
2600 mbsf
5000 mbsf

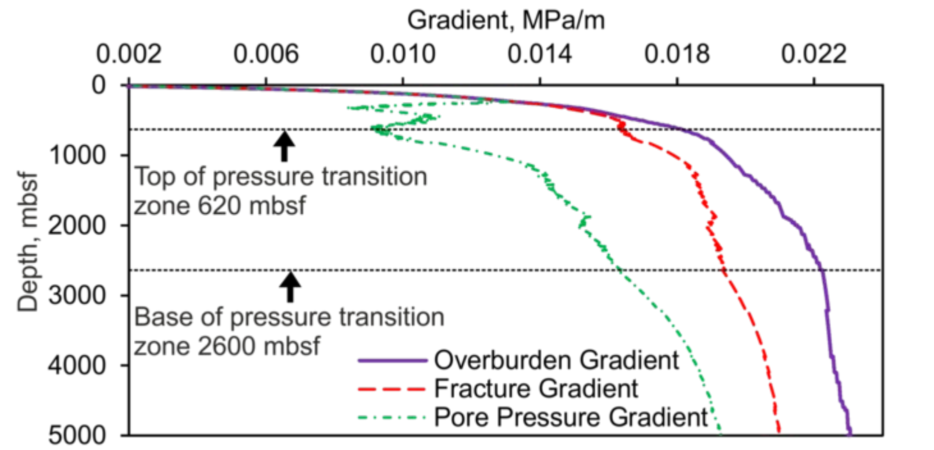

Gradient, MPa/m
0.002
0.006
0.010
0.014
0.018
0.022
0
1000
2000
3000
4000
5000
Depth, mbsf
Top of pressure transition
zone 620 mbsf
Base of pressure transition
zone 2600 mbsf
Overburden Gradient
Fracture Gradient
Pore Pressure Gradient

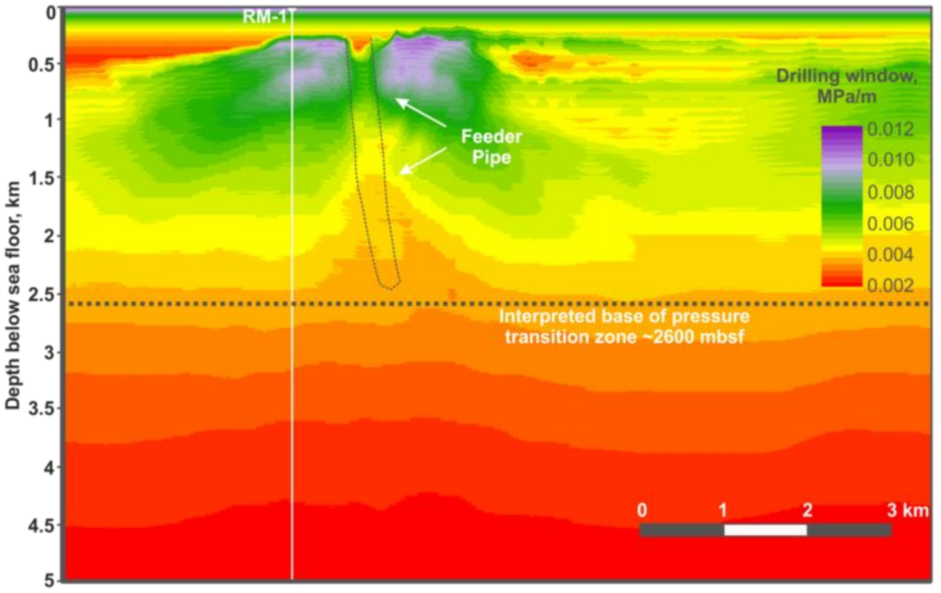

RM-1
Depth below sea floor, km
0
0.5
1
1.5
2
2.5
3
3.5
4
4.5
5
Feeder
Pipe
Drilling window,
MPa/m
0.012
0.010
0.008
0.006
0.004
0.002
Interpreted base of pressure
transition zone ~2600 mbsf
0
1
2
3 km

Table 1. *Analytical and empirical correlations employed in the study. V_p is km/s. Asterisks in the second column indicate that the relationship is analytical*

Type	#	PROPERTY		UNIT	EQUATION	NOTE	REFERENCE
Elastic parameters	1	Shear wave velocity	V_s	km/s	$0.8621V_p - 1.1724$	Mudrock line for clastics	Castagna et al. 1985, Eq. 1
	2	Bulk density	ρ_b	kg/m³	aV_p^m	Amended Gardner's equation for shales, where a=516.2 and m=0.1869	Quijada & Stewart 2007, Table 2
	3*	Porosity	ϕ	-	$(\rho_{matrix} - \rho_b)/(\rho_{matrix} - \rho_{fluid})$	ρ_{matrix} = 2600 kg/m³ and ρ_{fluid}=1000 kg/m³. Explanation follows Table 1	Avseth et al. 2010, p. 57, Eq. 2.10
	4	Theoretical porosity	ϕ_t	-	$\phi_0 e^{-\beta\sigma_v}$	?0 is the pre-compaction porosity. β=0.0421 and ?0=0.4	Rubey & Hubbert 1959, Eq. 16 Buryakovsky et al. 2001, p. 353, 374
	5*	Shear modulus	G	GPa	$\rho_b V_s^2$		Mavko et al. 2009, p. 81
	6*	Lamé's constant	λ	GPa	$\rho_b V_p^2 - 2G$		Mavko et al. 2009, p. 81
	7*	Poisson's ratio	ν	-	$(V_p^2 - 2V_s^2)/[2(V_p^2 - V_s^2)]$		Mavko et al. 2009, p. 81
	8*	Young's modulus	E	GPa	$G(3V_p^2 - 4V_s^2)/(V_p^2 - V_s^2)$		Mavko et al. 2009, p. 82
	9*	Bulk modulus	K	GPa	$\rho_b(3V_p^2 - 4V_s^2)/3$		Mavko et al. 2009, p. 82
In-situ stress and pressure	10*	Overburden stress	σ_v	MPa	$\rho_w g z_w + \rho_b g(z - z_w)$	ρ_w and z_w are the density and depth of the water, respectively	Zoback 2007, p. 8, Eq. 1.6
	11	Horizontal stress	σ_h	MPa	$\sigma_v \nu/(1-\nu)$	In the calculations we approximate σ_H~σ_h, where σ_H and σ_h are max. and min. horizontal stresses, respectively. Explanation of their permissible magnitudes follows Table 1	Iverson 1995, Eq. 4
	12*	Hydrostatic pressure	P_h	MPa	$\rho_w g z$		Zoback 2007, p. 28, Eq. 2.1
	13	Pore Fluid pressure	P_p	MPa	$\sigma_v - (1/\beta)\ln(\phi_0/\phi)$	Pressure existing in the pores of the formation. Derived from Eq. 4	Rubey & Hubbert 1959, Eq. 16
	14	Fracture pressure	P_f	MPa	$P_p + (\sigma_v - P_p)(\sigma_h/\sigma_v)$	Explanation follows Table 1	Mathews & Kelly 1967, p. 7
Strength properties	15	Friction angle	φ	°	$\sin^{-1}((V_p - 1)/(V_p + 1))$	For shales	Lal 1999, Eq. 17
	16	Cohesive strength	τ_0	MPa	$5(V_p - 1)/\sqrt{V_p}$	For shales	Lal 1999, Eq. 17
	17	Uniaxial Compressive Strength	C	MPa	$1.35V_p^{2.6}$	For shales, worldwide	Chang et al. 2006, Eq. 14

Table 2. *Feasibility model input parameters*

Structural position	Depth, m	P-wave velocity, km/s	S-wave velocity, km/s	Porosity, %
Crest	500	2.015	0.638	30
Flank	1500	2.591	1.076	17

Table 3. *Modelled values of elastic properties, state of stress and rock strength on the crest and flank of a mud volcano from the KAD structure*

Estimated parameters			Structural position		Values from the literature	
Type	**Name**	**Unit**	**Crest**	**Flank**	**Range**	**Reference**
Elastic properties	Bulk density	kg/m^3	2140	2243	1580 – 2600	Mavko et al. 2009, p. 458, 459
	Shear modulus	GPa	0.87	2.60	0.2-5.5	Horsrud 2001, p. 71
	Lamé's constant	GPa	8.69	15.06	0.07-13.26	Islam & Skalle 2013, p. 1400
	Poisson's ratio	-	0.44	0.40	0.35-0.50	Schön 2011, p 162
	Young's modulus	GPa	2.52	7.25	3.2 – 9.5	Prasad et al. 2012, p. 3
	Bulk modulus	GPa	7.53	11.59	6 – 12	Vanorio et al. 2003, p. 325
Stress and pressures	Vertical stress	MPa	13	35	10-35	Buryakovsky et al. 2001, p. 402
	Horizontal stress	MPa	8	22		
	Hydrostatic pressure	MPa	5	15	4-14	Buryakovsky et al. 2001, p. 402
	Pore fluid pressure	MPa	6	16	12 – 20	Buryakovsky et al. 2001, p. 152
	Fracture pressure	MPa	11.57	28.41		
Rock strength	Friction angle	°	19.67	26.30	21.75 – 38.09	Kohli & Zoback 2013, p. 5115
	Cohesive strength	MPa	3.58	4.94	0.3 – 38.4	Schön 2011, p. 256
	UCS	MPa	8.35	16.05	7.5 – 13.9	Schön 2011, p. 258

Table 4. *Input parameters and calculated minimum and maximum values of σ_h and σ_H respectively used to construct the stress polygons shown in Fig. 19. The stress and pressure values have been normalized by the corresponding depth*

Depth, m	σ_v, MPa/m	P_p, MPa/m	μ	σ_H, MPa/m	σ_h, MPa/m
620	0.0235	0.0123	0.3718	0.0356	0.0177
2600	0.0236	0.0174	0.5957	0.0369	0.0194
5000	0.0238	0.0200	0.6445	0.0328	0.0211